



Size-resolved CCN  
and HR-ToF-AMS  
measurements in  
Hong Kong

J. W. Meng et al.

This discussion paper is/has been under review for the journal Atmospheric Chemistry and Physics (ACP). Please refer to the corresponding final paper in ACP if available.

# Cloud condensation nuclei (CCN) and HR-ToF-AMS measurements at a coastal site in Hong Kong: size-resolved CCN activity and closure analysis

J. W. Meng<sup>1</sup>, M. C. Yeung<sup>2</sup>, Y. J. Li<sup>1</sup>, B. Y. L. Lee<sup>1</sup>, and C. K. Chan<sup>1,2</sup>

<sup>1</sup>Division of Environment, Hong Kong University of Science and Technology, Clear Water Bay, Hong Kong SAR, China

<sup>2</sup>Department of Chemical and Biomolecular Engineering, The Hong Kong University of Science and Technology Clear Water Bay, Hong Kong SAR, China

Received: 6 March 2014 – Accepted: 10 March 2014 – Published: 3 April 2014

Correspondence to: C. K. Chan (keckchan@ust.hk)

Published by Copernicus Publications on behalf of the European Geosciences Union.

Title Page

Abstract

Introduction

Conclusions

References

Tables

Figures



Back

Close

Full Screen / Esc

Printer-friendly Version

Interactive Discussion



## Abstract

The cloud condensation nuclei (CCN) properties of atmospheric aerosols were measured on 1–30 May 2011 at a coastal site in Hong Kong. Size-resolved CCN activation curves, the ratio of number concentration of CCN ( $N_{\text{CCN}}$ ) to aerosol concentration ( $N_{\text{CN}}$ ) as a function of particle size, were obtained at supersaturation (SS) = 0.15 %, 0.35 %, 0.50 %, and 0.70 % using a DMT CCN counter (CCNc) and a TSI scanning mobility particle sizer (SMPS). The mean bulk size-integrated  $N_{\text{CCN}}$  ranged from  $\sim 500 \text{ cm}^{-3}$  at SS = 0.15 % to  $\sim 2100 \text{ cm}^{-3}$  at SS = 0.70 %, and the mean bulk  $N_{\text{CCN}}/N_{\text{CN}}$  ratio ranged from 0.16 at SS = 0.15 % to 0.65 at SS = 0.70 %. The average critical mobility diameters ( $D_{50}$ ) at SS = 0.15 %, 0.35 %, 0.50 %, and 0.70 % were 116 nm, 67 nm, 56 nm, and 46 nm, respectively. The corresponding average hygroscopic parameters ( $\kappa_{\text{CCN}}$ ) were 0.39, 0.36, 0.31, and 0.28. The decrease in  $\kappa_{\text{CCN}}$  can be attributed to the increase in organic to inorganic volume ratio as particle size decreases, as measured by an Aerodyne high resolution time-of-flight aerosol mass spectrometer (HR-ToF-AMS). The  $\kappa_{\text{CCN}}$  correlates reasonably well with  $\kappa_{\text{AMS}}$  based on size-resolved AMS measurements:  $\kappa_{\text{AMS}} = \kappa_{\text{org}} \times f_{\text{org}} + \kappa_{\text{inorg}} \times f_{\text{inorg}}$ , where  $f_{\text{org}}$  and  $f_{\text{inorg}}$  are the organic and inorganic volume fractions, respectively,  $\kappa_{\text{org}} = 0.1$  and  $\kappa_{\text{inorg}} = 0.6$ , with a  $R^2$  of 0.51.

In closure analysis,  $N_{\text{CCN}}$  was estimated by integrating the measured size-resolved  $N_{\text{CN}}$  for particles larger than  $D_{50}$  derived from  $\kappa$  assuming internal mixing state. Estimates using  $\kappa_{\text{AMS}}$  from size-resolved AMS measurements show that the measured and predicted  $N_{\text{CCN}}$  were generally within 10 % of each other at all four SS. The deviation increased to 26 % when  $\kappa_{\text{AMS}}$  was calculated from bulk  $\text{PM}_{10}$  AMS measurements of particles because  $\text{PM}_{10}$  was dominated by particles of 200 nm to 500 nm in diameter, which had a larger inorganic fraction than those of  $D_{50}$  (particle diameter < 200 nm). A constant  $\kappa = 0.33$  (the average value of size-resolved  $\kappa_{\text{AMS}}$  over the course of campaign) was found to give an  $N_{\text{CCN}}$  prediction within 12 % of the actual measured values. We also compared  $N_{\text{CCN}}$  estimates based on the measured average  $D_{50}$  and the average size-resolved CCN activation ratio to examine the relative importance of hygroscopicity

ACPD

14, 9067–9107, 2014

## Size-resolved CCN and HR-ToF-AMS measurements in Hong Kong

J. W. Meng et al.

Title Page

Abstract

Introduction

Conclusions

References

Tables

Figures

⏪

⏩

◀

▶

Back

Close

Full Screen / Esc

Printer-friendly Version

Interactive Discussion

and mixing state.  $N_{\text{CCN}}$  was found to be relatively more sensitive to the mixing state and hygroscopicity at a high SS = 0.70 % and a low SS = 0.15 %, respectively.

## 1 Introduction

Atmospheric aerosols can act as cloud condensation nuclei (CCN) and affect cloud formation by influencing the CCN number concentration ( $N_{\text{CCN}}$ ) and the size of cloud droplets. Whether aerosol particles will eventually form cloud droplets under a set atmospheric condition mainly depends on their size, chemical composition, and mixing states. Predicting  $N_{\text{CCN}}$  usually involves measuring the aerosol size distribution and making assumptions about the chemical composition associated to mixing state. Bulk chemical compositions and an assumption of internal mixing state (i.e., particles are identical mixtures of all participating species) are often used in predicting  $N_{\text{CCN}}$  (Moore et al., 2012a; Wang et al., 2010). Ambient aerosols are complex mixtures and the aerosol compositions vary substantially with particle size. The hygroscopicity parameter ( $\kappa$ ) is used to represent the effect of chemical composition on CCN activity (Petters and Kreidenweis, 2007, 2013). Size-resolved chemical compositions give a size-dependent  $\kappa$  which leads to better  $N_{\text{CCN}}$  predictions than those based on bulk compositions (Medina et al., 2007; Stroud et al., 2007; Wang et al., 2010).

While the real-time aerosol size-resolved chemical compositions such as non-refractory (NR)-species and black carbon (BC) can be obtained with an aerosol mass spectrometer and a single particle soot photometer, respectively, information on the mixing state is usually not available or incomplete. Various assumptions have been applied to describe the aerosol mixing state (Asa-Awuku et al., 2011; Bougiatioti et al., 2009; Cubison et al., 2008; Ervens et al., 2010; Lance et al., 2009; Latham et al., 2013; Moore et al., 2012a; Rose et al., 2011; Wang et al., 2010).  $N_{\text{CCN}}$  predictions assuming internal mixing are usually larger than measured values by 20 % or even more, since this assumption overestimates the contribution of organics to  $N_{\text{CCN}}$  (Rose et al., 2011; Wang et al., 2010; Wex et al., 2010). Another extreme assumption is external mixing,

## Size-resolved CCN and HR-ToF-AMS measurements in Hong Kong

J. W. Meng et al.

Title Page

Abstract

Introduction

Conclusions

References

Tables

Figures



Back

Close

Full Screen / Esc

Printer-friendly Version

Interactive Discussion





## Size-resolved CCN and HR-ToF-AMS measurements in Hong Kong

J. W. Meng et al.

Title Page

Abstract

Introduction

Conclusions

References

Tables

Figures

⏪

⏩

◀

▶

Back

Close

Full Screen / Esc

Printer-friendly Version

Interactive Discussion

In this study, we report for the first time size-resolved measurements of CCN activity in Hong Kong. We correlated the CCN-derived hygroscopicity ( $\kappa_{\text{CCN}}$ ) with those estimated from the size-dependent aerosol chemical compositions determined by an Aerodyne high-resolution Time-of-Flight Aerosol Mass Spectrometer (HR-ToF-AMS, hereafter as AMS). Assuming internal mixtures, we carried out closure studies on  $N_{\text{CCN}}$  prediction based on the size-distributions of  $N_{\text{CN}}$  measured by a TSI SMPS and on the hygroscopicity values derived from size resolved and size integrated chemical compositions measured by AMS using Köhler theory,  $\kappa_{\text{AMS}}$ , and some assumed constants. Finally, using the average  $D_{50}$  and the size-resolved CCN activation ratios from the CCN measurements, we examined the relative importance of hygroscopicity and mixing state in  $N_{\text{CCN}}$  predictions at different SS.

## 2 Experimental methods

### 2.1 Sampling site and meteorological conditions

Measurements of aerosol chemical properties and CCN activity were carried out throughout the entire month of May 2011 at the Air Quality Research Supersite situated on the campus of the Hong Kong University of Science and Technology (HKUST) on the east coast of Hong Kong (see <http://www.envr.ust.hk/research/research-facility/background-materials.html>). High relative humidity (RH) with a mean of 81 % and an average temperature of 26.0 °C prevailed in this study. More information on the sampling location and meteorological conditions is available from Lee et al. (2013) and Li et al. (2013).

## 2.2 Instrument setup

### 2.2.1 Sample inlet system

Ambient air was sampled at a flow rate of  $16.67 \text{ L min}^{-1}$  after passing through a  $\text{PM}_{2.5}$  cyclone on the roof of the Supersite (appropriately 20 m a.s.l.) and into a stainless steel sampling port supplying the on-line instruments of the TSI SMPS, the Droplet Measurement Technologies (DMT) dual column continuous-flow CCN counter (CCNc-200) and the Aerodyne AMS. The sampled air passed through a 1 m long diffusion drier (BMI, San Francisco, CA) filled with silica gel, thus its RH was below 30 % before it went into the above instruments for measurements.

### 2.2.2 CCN measurements

Size-resolved CCN spectra and activation ratios were measured with the CCNc-200 (Lance et al., 2006; Roberts and Nenes, 2005) coupled with a TSI SMPS, consisting of a differential mobility analyzer (DMA, TSI 3081L) and a water-based condensation particle counter (WCPC, TSI 3785).

As shown in Fig. 1, charge-neutralized aerosols passed through the DMA for classification. The classified aerosols were then split into two streams: with one going into the WCPC for  $N_{\text{CN}}$  measurements and the other into the CCNc-200 for  $N_{\text{CCN}}$  measurements. The particle size distribution was measured every 6 min, with an up-scan time of 300 s. The sample flow rate was  $1 \text{ L min}^{-1}$  for the DMA,  $0.5 \text{ L min}^{-1}$  for the WCPC and the CCNc-200 each, and the closed-loop sheath air flow rate was  $10 \text{ L min}^{-1}$ . These flow rate settings allow SMPS (DMA + WCPC) measurements for particles ranging from 7 nm to 300 nm in mobility diameter ( $D_m$ ), which as we will show later, cover the  $D_{50}$  ( $D_m$ ) range of the particles studied. The sheath flow rate was continuously corrected using a mass flow controller. All flow rates were regularly checked and sizing accuracy for the SMPS and the CCNc-200 was verified with Polystyrene latex (PSL) spheres.

## Size-resolved CCN and HR-ToF-AMS measurements in Hong Kong

J. W. Meng et al.

Title Page

Abstract

Introduction

Conclusions

References

Tables

Figures

⏪

⏩

◀

▶

Back

Close

Full Screen / Esc

Printer-friendly Version

Interactive Discussion



## Size-resolved CCN and HR-ToF-AMS measurements in Hong Kong

J. W. Meng et al.

Title Page

Abstract

Introduction

Conclusions

References

Tables

Figures

⏪

⏩

◀

▶

Back

Close

Full Screen / Esc

Printer-friendly Version

Interactive Discussion

The CCNc-200 was operated at a total flow rate of  $1 \text{ Lmin}^{-1}$ , of which  $0.5 \text{ Lmin}^{-1}$  was for column A connected to the DMA to measure the size-resolved CCN spectrum and another  $0.5 \text{ Lmin}^{-1}$  was for column B connected to the sample inlet system to measure the total  $N_{\text{CCN}}$ . A sheath-to-aerosol flow ratio of 10 was used. Lathem and Nenes (2011) pointed out that the direct measurements could lead to underestimations of bulk  $N_{\text{CCN}}$  due to the depletion of water inside the column by a large amount of aerosols and recommended the use of size-resolved CCN measurement. In our measurements, the bulk  $N_{\text{CCN}}$  integrated from size-resolved CCN measurement using column A are usually fewer than  $5000 \text{ cm}^{-3}$  and they correlate well with that from the direct measurement using column B with a slope of 0.97 and correlation coefficient ( $R^2$ ) of 0.53 as shown in Fig. S1. We use bulk  $N_{\text{CCN}}$  calculated from column A for the comparison with  $N_{\text{CN}}$  from SMPS and for the closure study below. For every measurement cycle, four SS (0.15 %, 0.35 %, 0.50 %, and 0.70 %) were selected. Measurements at SS = 0.15 % lasted 22 min whereas those at other SS lasted 12 min each for repeatability. CCNc temperature transients during SS changes are known to produce unreliable spectra if they occur during a voltage up-scan (Moore et al., 2010). In our measurements, the instrument profiles were allowed up to  $\sim 2$  min to stabilize whenever the temperature gradient was changed. At SS = 0.15 %, a longer time ( $\sim 4$  min) was required for the stabilization of temperatures. Only data collected under stabilized temperatures were used for analysis.

The CCNc-200 was calibrated with size selected DMA ammonium sulfate particles at the four SS (Deng et al., 2011; Rose et al., 2008) regularly during the campaign. The instrument SS was derived from Köhler theory using a constant van't Hoff factor of 2.5 for ammonium sulfate (Low, 1969; Tang and Munkelwitz, 1994; Young and Warren, 1992).

## 2.2.3 Aerosol chemical compositions

Non-refractory PM<sub>1</sub> (NR-PM<sub>1</sub>) constituents of sulfate, nitrate, ammonium, chloride, and organics were measured with the AMS operated under V, pToF, and W modes. The principle behind the instrument has been described in detail elsewhere (DeCarlo et al., 2006) and will only be briefly described here. In pToF mode, the instrument performs particle sizing based on particle time-of-flight with the aid of a chopper and gives size-resolved chemical composition data in vacuum aerodynamic diameter ( $D_{va}$ ) (DeCarlo et al., 2004). In V mode, the shorter traveling path for ions in the ion time-of-flight (ToF) chamber gives a mass spectral resolving power of approximately 2000 (DeCarlo et al., 2006) and better sensitivity. In W mode, the mass spectral resolving power is approximately 4000 (DeCarlo et al., 2006) but the signal-to-noise ratio is lower. The instrument was operated alternately between the V + pToF combined mode and the W mode for 5 min each. Evaluation of the ionization efficiency (IE) was carried out with ammonium nitrate particles weekly and both the flow rate and particle sizing were calibrated before and after the campaign. A more detailed description of the performance of the AMS during the campaign is presented by Li et al. (2013) and Lee et al. (2013). The AMS only measures NR-species but not elemental carbon (EC), sea salt, or crustal species. However, EC only accounts for less than 5% of the PM<sub>1</sub> mass and hence can be neglected (Huang et al., 2014; Lee et al., 2013). Sea salt and crustal species typically exist in the coarse mode and make negligible contributions to PM<sub>1</sub>.

## 2.3 Data analysis

### 2.3.1 CN and CCN data

The time series of  $N_{CN}$  and  $N_{CCN}$  distributions were obtained using the TSI Aerosol Instrument Manager (AIM) software (Wang and Flagan, 1989) and CCN acquisition software, respectively. The data collected during the voltage up-scan were employed for the inversion. The Scanning Mobility CCN Analysis (SMCA) was employed for

ACPD

14, 9067–9107, 2014

## Size-resolved CCN and HR-ToF-AMS measurements in Hong Kong

J. W. Meng et al.

Title Page

Abstract

Introduction

Conclusions

References

Tables

Figures

⏪

⏩

◀

▶

Back

Close

Full Screen / Esc

Printer-friendly Version

Interactive Discussion

calculating the size-resolved CCN activation fractions (Moore et al., 2010). The ratio of  $N_{CCN}$  to  $N_{CN}$  gives the size-resolved CCN activation fraction at each size. Then, the size-resolved CCN activation ratio was obtained by fitting the activation fraction with the sigmoidal function described by Eq. (1) (see Sect. 2.3.3) (Moore et al., 2010; Padró et al., 2010).

### 2.3.2 HR-ToF-AMS data

The standard toolkit of SQUIRREL (Sueper, 2011) was used for AMS data analysis. The collection efficiency (CE) used for this work was 0.5 and the relative ionization efficiency (RIE) of 1.2 for sulfate, 1.1 for nitrate, 1.3 for chloride, 1.4 for organics and 4.0 for ammonium were used as described by Li et al. (2013) and Lee et al. (2013). The size-resolved mass spectra for vacuum aerodynamic diameter ( $D_{va}$ ) ranging from 50 nm to 2000 nm (DeCarlo et al., 2004) were obtained every 5 min on average. The mass concentration of each size bin was obtained by averaging with the two adjacent size bins to reduce the influence of noise (Rose et al., 2011). In order to relate the size-resolved AMS data with those of SMPS and CCNc measurements directly, the AMS  $D_{va}$  size was divided by a factor of 1.7 to obtain the corresponding mobility equivalent diameter ( $D_m$ ) (Cheng et al., 2006; DeCarlo et al., 2004; Lee et al., 2013). The volume fractions of size-resolved chemical compositions were calculated from the mass concentrations using densities of organics and inorganics of  $1.3 \text{ g cm}^{-3}$  and  $1.75 \text{ g cm}^{-3}$ , respectively (Alfarra et al., 2006; Cross et al., 2007; Gunthe et al., 2009; King et al., 2007; Lee et al., 2013).

### 2.3.3 $D_{50}$ , $\kappa_{CCN}$ and $\kappa_{AMS}$

The critical diameter  $D_{50}$ , also known as the activation diameter, is the diameter at which 50% of the particles are activated at a specific SS. The  $D_{50}$  of a simple sigmoidal shaped activation ratio curve is determined by fitting the size-resolved activation

## Size-resolved CCN and HR-ToF-AMS measurements in Hong Kong

J. W. Meng et al.

Title Page

Abstract

Introduction

Conclusions

References

Tables

Figures

⏪

⏩

◀

▶

Back

Close

Full Screen / Esc

Printer-friendly Version

Interactive Discussion

fractions with the equation below:

$$\frac{N_{\text{CCN}}}{N_{\text{CN}}} = \frac{B}{\left(1 + \frac{D_p}{D_{50}}\right)^c} \quad (1)$$

where  $D_p$  is the dry mobility diameter,  $B$ ,  $c$ , and  $D_{50}$  are fitting coefficients that describe the asymptote/plateau, the slope, and the inflection point of the sigmoid, respectively (Moore et al., 2010; Padró et al., 2012). The values of  $B$  were more than 90 % during the whole campaign, indicating most of the particles were in the internal mixing state (Mei et al., 2013).

The measured hygroscopic parameter ( $\kappa_{\text{CCN}}$ ) is determined from  $D_{50}$  by:

$$\kappa_{\text{CCN}} = \frac{4A^3 \sigma_{\text{s/a}}^3(T)}{27T^3 D_{50}^3 \ln^2 S_c} \quad (2)$$

where  $A = 8.69251 \times 10^{-6} \text{ Km}^3 \text{ J}^{-1}$ ,  $\sigma_{\text{s/a}}(T)$  is the temperature-dependent surface tension of the solution/air interface,  $T$  is temperature and  $S_c$  is the critical saturation ratio. Pure water surface tension is assumed in the calculations of  $\kappa_{\text{CCN}}$  in this paper (Petters and Kreidenweis, 2013; Sullivan et al., 2009).

The hygroscopic parameter  $\kappa_{\text{AMS}}$  can be obtained from AMS measurements using

$$\kappa_{\text{AMS}} = \sum_i^n f_i \kappa_i \quad (3)$$

where  $f_i$  and  $\kappa_i$  are the size-resolved volume fraction derived from AMS measurements and the hygroscopic parameter of the species  $i$ , respectively (Petters and Kreidenweis, 2007). In this study, the Eq. (3) is simplified as:

$$\kappa_{\text{AMS}} = \kappa_{\text{org}} \times f_{\text{org}} + \kappa_{\text{inorg}} \times f_{\text{inorg}} \quad (4)$$

## 3 Results and discussion

### 3.1 Overview

Figure 2 shows an overview of the bulk  $N_{\text{CCN}}$  concentrations and  $N_{\text{CCN}}/N_{\text{CN}}$  activation ratio at SS of (a) 0.15 %, (b) 0.35 %, (c) 0.50 %, and (d) 0.70 %, as well as (e) the bulk  $N_{\text{CN}}$  and the NR-PM<sub>1</sub> total and component mass concentration and (f) the volume fractions of the AMS chemical components over the entire month of May 2011. Statistics of the measurements are given in Table 1. The gaps in the data in Fig. 2 are due to instrument downtime. For most of the time, the total  $N_{\text{CCN}}$  at SS of 0.15 %, 0.35 %, 0.50 % and 0.70 % were below  $800 \text{ cm}^{-3}$ ,  $3000 \text{ cm}^{-3}$ ,  $5000 \text{ cm}^{-3}$  and  $5600 \text{ cm}^{-3}$  respectively, and  $N_{\text{CN}}$  was below  $10\,000 \text{ cm}^{-3}$ . Both  $N_{\text{CCN}}$  and  $N_{\text{CN}}$  in this study are lower than those observed in July 2006 in Guangzhou (Rose et al., 2010). Large fluctuations in the bulk  $N_{\text{CCN}}/N_{\text{CN}}$  ratios were also observed. The bulk  $N_{\text{CCN}}/N_{\text{CN}}$  ratio was as low as 0.03 at SS = 0.15 %, but it was as high as 0.92 at SS = 0.70 %. Even at the same SS, the bulk  $N_{\text{CCN}}$ ,  $N_{\text{CN}}$  and  $N_{\text{CCN}}/N_{\text{CN}}$  ratio varied greatly during the campaign.

The bulk mass concentrations of NR-PM<sub>1</sub> ranged from  $0.8 \mu\text{g m}^{-3}$  to  $72.4 \mu\text{g m}^{-3}$  with a mean value of  $14.5 \pm 9.7 \mu\text{g m}^{-3}$  as shown in Fig. 2e. The average bulk volume fractions of NR-species were  $53 \pm 10 \%$ ,  $25 \pm 13 \%$ ,  $18 \pm 4 \%$ ,  $4 \pm 3 \%$  for sulfate, organics, ammonia, and nitrate, respectively (Lee et al., 2013). The bulk mass concentrations for all NR-species were in general low during the campaign compared with those reported for the PRD region (Gong et al., 2012; Rose et al., 2011; Takegawa et al., 2009; Xiao et al., 2011).

There were two periods of particular interest during this campaign: one was a foggy period (15 May) and the other was a hazy period (28–30 May). During the foggy period, the average RH was 91 % and the bulk NR-PM<sub>1</sub> was as high as  $30 \mu\text{g m}^{-3}$  (Fig. 2e; Li et al., 2013). The hazy period saw the highest mass concentration of NR-PM<sub>1</sub> species recorded during the whole campaign, but the RH was relatively low (66 %). The highest degree of oxygenation of organic aerosol (OA) with O : C ratio = 0.51 and fraction of

ACPD

14, 9067–9107, 2014

## Size-resolved CCN and HR-ToF-AMS measurements in Hong Kong

J. W. Meng et al.

Title Page

Abstract

Introduction

Conclusions

References

Tables

Figures

⏪

⏩

◀

▶

Back

Close

Full Screen / Esc

Printer-friendly Version

Interactive Discussion



ranged from 0.73 at 42 nm to 0.25 at 200 nm. Additionally, the bulk volume ratio of organics to inorganics between 42 nm and 200 nm was 0.65 in the foggy period, 1.33 in the hazy period, and 0.87 in the non-episode periods.

The measured  $\kappa_{\text{CCN}}$  (yellow symbols) and the calculated  $\kappa_{\text{AMS}}$  (blue symbols), in the form of median values and interquartile ranges, are plotted against their corresponding  $D_{50}$  in Fig. 3d–f. The median and mean values of  $\kappa_{\text{CCN}}$  and  $\kappa_{\text{AMS}}$  were essentially the same. Overall, the median  $D_{50}$  were 116 nm, 68 nm, 55 nm, and 47 nm, with an interquartile range of less than 16 %, at SS of 0.15 %, 0.35 %, 0.50 %, and 0.70 %, respectively. During the foggy period, which featured high inorganics volume fractions, the median  $\kappa_{\text{CCN}}$  were 0.44, 0.37, 0.36 and 0.29 at SS from 0.15 % to 0.70 %. They are higher than the corresponding values in the hazy period (0.38, 0.36, 0.32 and 0.28) and the non-episode periods (0.39, 0.37, 0.33 and 0.27). The difference in  $\kappa_{\text{CCN}}$  was most obvious at SS = 0.15 %, at which  $D_{50}$  was around 110 nm, and the corresponding inorganic volume fraction was 0.6 in foggy period, 0.4 in the hazy period and 0.5 in the non-episode period. The high inorganic volume fraction results in high aerosol hygroscopicity.

The  $\kappa_{\text{AMS}}$  calculated from Eq. (3) assuming  $\kappa_{\text{org}} = 0.1$  and  $\kappa_{\text{inorg}} = 0.6$  agreed well with the measured  $\kappa_{\text{CCN}}$  in the foggy period and the non-episode periods as shown in Fig. 3d and f. In the hazy period (Fig. 3e), assuming  $\kappa_{\text{org}} = 0.2$  and  $\kappa_{\text{inorg}} = 0.6$  gave better agreement between  $\kappa_{\text{AMS}}$  and  $\kappa_{\text{CCN}}$ , which can be explained by a high degree of oxygenation of aerosols with O : C ratio up to 0.51 for the organics species observed (Li et al., 2013), leading to a high hygroscopicity (Chang et al., 2010; Lambe et al., 2011; Massoli et al., 2010; Mei et al., 2013; Moore et al., 2012b).

We further examine the correlations between the observed  $\kappa_{\text{CCN}}$  and the size-resolved organic volume fraction ( $f_{\text{org}}$ ) in Fig. 4a for the hazy period and Fig. 4b for the rest of the campaign. In order to avoid the negatively impact of low signal-to-noise ratios of AMS measurements on the correlation study, only data points with mass concentrations in a size bin of larger than  $0.6 \mu\text{g m}^{-3}$  were used. Extrapolation of the least square fit line in Fig. 4a and b to  $f_{\text{org}} = 1$  yields  $\kappa_{\text{org}} = 0.21 \pm 0.02$  and  $0.09 \pm 0.01$  for the

## Size-resolved CCN and HR-ToF-AMS measurements in Hong Kong

J. W. Meng et al.

Title Page

Abstract

Introduction

Conclusions

References

Tables

Figures

◀

▶

◀

▶

Back

Close

Full Screen / Esc

Printer-friendly Version

Interactive Discussion



average  $D_{50}$  with an internal mixing assumption and the size-resolved CCN activation ratios from CCN measurements which reflect the actual mixing state of the aerosols. The last approach involved integrating the product of the measured size-distribution of  $N_{\text{CN}}$  and the size-resolved CCN activation ratio in each particle size bin.

### 5 3.3.1 Prediction of $N_{\text{CCN}}$ based on $\kappa_{\text{AMS}}$

#### $\kappa_{\text{AMS}}$ from bulk AMS measurements

The hygroscopicity  $\kappa_{\text{AMS}}$  was estimated by assuming that all particles have the same chemical composition as determined by bulk AMS measurements and  $\kappa_{\text{org}} = 0.1$  and  $\kappa_{\text{inorg}} = 0.6$ . The closure results are shown in Fig. 5 and Table 4. Overall, the approaches of using individual  $D_{50}$  and the average  $D_{50}$  grossly over-predicted  $N_{\text{CCN}}$  by up to 21 % and 26 %, respectively. As shown in Fig. 3a–c,  $\text{PM}_{10}$  was dominated by inorganic species with the bulk volume fraction as high as 69 % during the whole period. The bulk volume ratio mainly reflects the composition of particles from 200 to 500 nm where inorganic species dominated. On the other hand,  $D_{50}$  at the four SS were all less than 200 nm where organic species accounted for more than 39 % of bulk volume fraction as shown in Table 2 and Fig. 3. Therefore, deriving  $\kappa_{\text{AMS}}$  from bulk AMS measurements leads to a positive bias toward inorganic species, and hence an overestimation of  $\kappa_{\text{AMS}}$  and  $N_{\text{CCN}}$ . Wang et al. (2010) found that the overestimation arising from the use of the bulk mass concentrations decreased from 80 % to 39 % when SS decreased from 0.35 % to 0.11 %. Our data also shows decreasing overestimation as SS decreases, except for data at SS = 0.15 %, where the  $N_{\text{CCN}}$  was smaller than  $1000 \text{ cm}^{-3}$  most of the time. The low counts may have introduced larger uncertainty in the measurements as shown in SI.

## Size-resolved CCN and HR-ToF-AMS measurements in Hong Kong

J. W. Meng et al.

Title Page

Abstract

Introduction

Conclusions

References

Tables

Figures

⏪

⏩

◀

▶

Back

Close

Full Screen / Esc

Printer-friendly Version

Interactive Discussion



## $\kappa_{\text{AMS}}$ from size-resolved AMS measurements

Figure 6a–d and e–h show the correlations between the measured  $N_{\text{CCN}}$  and the  $N_{\text{CCN}}$  predicted from the individual  $D_{50}$  of each data set and the averaged  $D_{50}$  derived from size-resolved  $\kappa_{\text{AMS}}$ , respectively. The slope and  $R^2$  are given in Table 4. In general, the  $N_{\text{CCN}}$  prediction deviated by 10 % or less for both approaches and the average  $D_{50}$  adequately reflects the aerosol activation properties. At SS = 0.70 %, individual  $D_{50}$  and the average  $D_{50}$  gave the close deviations of 10 % and 9 % respectively between the measured and predicted  $N_{\text{CCN}}$ . At high SS, where even particles of moderate hygroscopicity are activated (Kim et al., 2011), the  $N_{\text{CCN}}$  prediction is less sensitive to hygroscopicity than at low SS. The difference of the deviations increased as SS decreased from 0.70 % to 0.35 %. At lower SS, differences in hygroscopicity as reflected from the different  $D_{50}$  used in the calculations gave larger differences in  $N_{\text{CCN}}$  predictions.

The overestimation from using the average  $D_{50}$  decreased from 9 % at SS of 0.70 % ( $D_{50} = 46$  nm) to 5 % and 1 % at SS of 0.50 % ( $D_{50} = 56$  nm) and 0.35 % ( $D_{50} = 67$  nm), respectively. The fraction of non/less-hygroscopic hydrocarbon-like organic aerosols (HOA) decreased with increasing particle size (Lee et al., 2013). They contribute little to  $N_{\text{CCN}}$  by themselves but the assumption of internal mixing allows them to contribute to CCN due to their mixing with more hygroscopic species and leads to an overestimated  $N_{\text{CCN}}$  (Rose et al., 2011; Wang et al., 2010). When SS decreased,  $D_{50}$  increased and the impact of HOA on the  $N_{\text{CCN}}$  predictions decreased because of their smaller abundance relative to the hygroscopic inorganics. The large deviation in  $N_{\text{CCN}}$  prediction at SS = 0.15 % may be due to the uncertainty in the low number counts of CCN measurements or the high sensitivity of  $N_{\text{CCN}}$  to hygroscopicity at low SS as discussed later.

### 3.3.2 Prediction of $N_{\text{CCN}}$ from the constant $\kappa$

A constant  $\kappa = 0.30$  has been proposed for predicting  $N_{\text{CCN}}$  and understanding the indirect effects of continental aerosols on climate on a global modeling scale (Andreae and

ACPD

14, 9067–9107, 2014

## Size-resolved CCN and HR-ToF-AMS measurements in Hong Kong

J. W. Meng et al.

Title Page

Abstract

Introduction

Conclusions

References

Tables

Figures

⏪

⏩

◀

▶

Back

Close

Full Screen / Esc

Printer-friendly Version

Interactive Discussion



## Size-resolved CCN and HR-ToF-AMS measurements in Hong Kong

J. W. Meng et al.

Title Page

Abstract

Introduction

Conclusions

References

Tables

Figures

⏪

⏩

◀

▶

Back

Close

Full Screen / Esc

Printer-friendly Version

Interactive Discussion

Rosenfeld, 2008; Pringle et al., 2010). Rose et al. (2011) showed that the deviations between the measured and predicted  $N_{\text{CCN}}$  were less than 20 % when they used an averaged  $\kappa = 0.30$  over the course of their campaign in PRD in 2006. We evaluated the use of constant  $\kappa = 0.30$ , 0.33 (the average size-resolved  $\kappa_{\text{AMS}}$  over the campaign at the four SS), and 0.35 to estimate  $N_{\text{CCN}}$ . Overall, using  $\kappa = 0.35$  overestimated  $N_{\text{CCN}}$  at all four SS while using 0.33 and 0.30 underestimated it at low  $\text{SS} \leq 0.35\%$  and overestimated it at high  $\text{SS} \geq 0.50\%$ , respectively, as shown in Fig. S3 and Table 4. The slopes for  $\kappa = 0.30$ , 0.33 and 0.35 are quite different (0.91, 0.98 and 1.05) at  $\text{SS} = 0.15\%$ , while they are much closer (1.11, 1.12 and 1.13) at  $\text{SS} = 0.70\%$ . The difference in  $N_{\text{CCN}}$  prediction for the three  $\kappa$  decreased gradually from 14 % at  $\text{SS} = 0.15\%$  to 2 % at  $\text{SS} = 0.70\%$ . These results further confirm that the prediction of  $N_{\text{CCN}}$  is less sensitive to  $\kappa$  at high SS than at low one, and that the impact of hygroscopicity on the  $N_{\text{CCN}}$  prediction decreases with increasing SS.

The difference in the sensitivity of predicted  $N_{\text{CCN}}$  to hygroscopicity at different SS can also be attributed to the aerosol size distributions (Dusek et al., 2006; Ervens et al., 2007). The average aerosol size distribution over the whole period had a main mode at  $\sim 70$  nm and a shoulder at  $\sim 30$  nm (Fig. 7a) in this campaign. At  $\text{SS} = 0.15\%$ ,  $D_{50}$  is approximately 116 nm and on the right of the main mode (Fig. 7b), a slight variation of  $\kappa$  and  $D_{50}$  will cause a large change in  $N_{\text{CCN}}$  prediction. On the contrary, at  $\text{SS} = 0.70\%$ , the corresponding  $D_{50} = 46$  nm is on the left of the main mode (Fig. 7c), a variation of  $\kappa$  and  $D_{50}$  will have less impact on  $N_{\text{CCN}}$  prediction as the  $N_{\text{CCN}}$  is dominated by the mode at 70 nm.

In addition, we carried out the  $N_{\text{CCN}}$  prediction during the hazy period, when HOA contributes to  $\sim 25\%$  of OA (Li et al., 2013), based on the average size-resolved (1)  $\kappa_{\text{AMS}} = 0.33$  over the whole campaign period and (2)  $\kappa_{\text{AMS}} = 0.35$  over the hazy period only. As shown in Fig. S4, using  $\kappa_{\text{AMS}} = 0.33$  and 0.35 gave similar results with overestimations of 14 % and 13 % at  $\text{SS} = 0.70\%$  respectively. In the hazy period, the assumption of internal mixing state allowed HOA containing particles to act as CCN, thereby resulting in an overestimation of  $N_{\text{CCN}}$  by up to 14 %. At  $\text{SS} = 0.15\%$ , using

$\kappa = 0.33$  led to an overestimation of just 2 %, while an overestimation of 9 % was found when using  $\kappa = 0.35$ . Overall, using  $\kappa = 0.33$  gave predictions of  $N_{\text{CCN}}$  (Table 4) comparable to those using the size-resolved  $\kappa_{\text{AMS}}$  and better than those using  $\kappa$  from bulk AMS measurement at all four SS.

### 3.3.3 Mixing state and hygroscopicity

As discussed earlier, closure analysis based on hygroscopicity or  $D_{50}$  derived from chemical compositions alone cannot account for variability in the mixing state of aerosols, which could cause significant differences between predicted and measured  $N_{\text{CCN}}$ . In this section, we first calculate  $N_{\text{CCN}}$  by integrating the measured size-resolved  $N_{\text{CN}}$  distributions above the average  $D_{50}$ , obtained from the average CCN size-resolved activation ratio over the whole campaign. The second method involves integrating the product of the measured size-distribution of  $N_{\text{CN}}$  and the average size-resolved CCN activation ratio in each particle size bin. The size-resolved  $N_{\text{CCN}}/N_{\text{CN}}$  activation ratios reflect the influences of both the size-resolved chemical compositions and mixing state on CCN activity, and thus can potentially be used to examine the relative importance of mixing state and hygroscopicity in closure analysis when compared to predictions assuming internal mixing state (Deng et al., 2013). The first method involves the hygroscopicity of aerosols as reflected by the value of  $D_{50}$  and the assumption of internal mixing while the second method involves hygroscopicity with actual mixing state information imbedded in the measured activation ratio curves. A comparison of the predictions of these two methods would give hints to the role of assumption of mixing states. The average size-resolved CCN activation ratios at the four SS over the whole campaign are shown in Fig. S5. Data points are shown as means  $\pm$  standard deviations.

The correlations of measured and predicted  $N_{\text{CCN}}$  based on the average  $D_{50}$  (a–d) and the average size-resolved activation ratio (e–h) are shown in Fig. 8. The slopes of the fitted lines and  $R^2$  at different SS are given in Table 4. The predicted and the measured  $N_{\text{CCN}}$  differed by less than 10 % using the average  $D_{50}$ . The difference is comparable to those using the average  $D_{50}$  from size-resolved  $\kappa_{\text{AMS}}$  (Fig. 6e–h). At

## Size-resolved CCN and HR-ToF-AMS measurements in Hong Kong

J. W. Meng et al.

Title Page

Abstract

Introduction

Conclusions

References

Tables

Figures

◀

▶

◀

▶

Back

Close

Full Screen / Esc

Printer-friendly Version

Interactive Discussion







## References

- Alfarra, M. R., Paulsen, D., Gysel, M., Garforth, A. A., Dommen, J., Prévôt, A. S. H., Worsnop, D. R., Baltensperger, U., and Coe, H.: A mass spectrometric study of secondary organic aerosols formed from the photooxidation of anthropogenic and biogenic precursors in a reaction chamber, *Atmos. Chem. Phys.*, 6, 5279–5293, doi:10.5194/acp-6-5279-2006, 2006.
- Andreae, M., O. and Rosenfeld, D.: Aerosol–cloud–precipitation interactions. Part 1. The nature and sources of cloud-active aerosols, *Earth-Sci. Rev.*, 89, 13–41, 2008.
- Asa-Awuku, A., Nenes, A., Gao, S., Flagan, R. C., and Seinfeld, J. H.: Water-soluble SOA from Alkene ozonolysis: composition and droplet activation kinetics inferences from analysis of CCN activity, *Atmos. Chem. Phys.*, 10, 1585–1597, doi:10.5194/acp-10-1585-2010, 2010.
- Asa-Awuku, A., Moore, R. H., Nenes, A., Bahreini, R., Holloway, J. S., Brock, C. A., Middlebrook, A. M., Ryerson, T. B., Jimenez, J. L., and DeCarlo, P. F.: Airborne cloud condensation nuclei measurements during the 2006 Texas Air Quality Study, *J. Geophys. Res.-Atmos.*, 116, D11201, doi:10.1029/2010jd014874, 2011.
- Bougiatioti, A., Fountoukis, C., Kalivitis, N., Pandis, S. N., Nenes, A., and Mihalopoulos, N.: Cloud condensation nuclei measurements in the marine boundary layer of the Eastern Mediterranean: CCN closure and droplet growth kinetics, *Atmos. Chem. Phys.*, 9, 7053–7066, doi:10.5194/acp-9-7053-2009, 2009.
- Chan, C. K. and Yao, X.: Air pollution in mega cities in China, *Atmos. Environ.*, 42, 1–42, 2008.
- Chang, R. Y.-W., Slowik, J. G., Shantz, N. C., Vlasenko, A., Liggio, J., Sjostedt, S. J., Leaitch, W. R., and Abbatt, J. P. D.: The hygroscopicity parameter ( $\kappa$ ) of ambient organic aerosol at a field site subject to biogenic and anthropogenic influences: relationship to degree of aerosol oxidation, *Atmos. Chem. Phys.*, 10, 5047–5064, doi:10.5194/acp-10-5047-2010, 2010.
- Cheng, Y. F., Eichler, H., Wiedensohler, A., Heintzenberg, J., Zhang, Y. H., Hu, M., Herrmann, H., Zeng, L. M., Liu, S., and Gnauk, T.: Mixing state of elemental carbon and non-light-absorbing aerosol components derived from in situ particle optical properties at Xinken in Pearl River Delta of China, *J. Geophys. Res.-Atmos.*, 111, D20204, doi:10.1029/2005jd006929, 2006.
- Cross, E. S., Slowik, J. G., Davidovits, P., Allan, J. D., Worsnop, D. R., Jayne, J. T., Lewis<sup>†</sup>, D. K., Canagaratna, M., and Onasch, T. B.: Laboratory and ambient particle density determinations

### Size-resolved CCN and HR-ToF-AMS measurements in Hong Kong

J. W. Meng et al.

Title Page

Abstract

Introduction

Conclusions

References

Tables

Figures

⏪

⏩

◀

▶

Back

Close

Full Screen / Esc

Printer-friendly Version

Interactive Discussion



**Size-resolved CCN  
and HR-ToF-AMS  
measurements in  
Hong Kong**

J. W. Meng et al.

Title Page

Abstract

Introduction

Conclusions

References

Tables

Figures

◀

▶

◀

▶

Back

Close

Full Screen / Esc

Printer-friendly Version

Interactive Discussion

using light scattering in conjunction with aerosol mass spectrometry, *Aerosol Sci. Tech.*, 41, 343–359, 2007.

Cubison, M. J., Ervens, B., Feingold, G., Docherty, K. S., Ulbrich, I. M., Shields, L., Prather, K., Hering, S., and Jimenez, J. L.: The influence of chemical composition and mixing state of Los Angeles urban aerosol on CCN number and cloud properties, *Atmos. Chem. Phys.*, 8, 5649–5667, doi:10.5194/acp-8-5649-2008, 2008.

DeCarlo, P. F., Slowik, J. G., Worsnop, D. R., Davidovits, P., and Jimenez, J. L.: Particle morphology and density characterization by combined mobility and aerodynamic diameter measurements. Part 1: Theory, *Aerosol Sci. Tech.*, 38, 1185–1205, 2004.

DeCarlo, P. F., Kimmel, J. R., Trimborn, A., Northway, M. J., Jayne, J. T., Aiken, A. C., Gonin, M., Fuhrer, K., Horvath, T., Docherty, K. S., Worsnop, D. R., and Jimenez, J. L.: Field-deployable, high-resolution, time-of-flight aerosol mass spectrometer, *Anal. Chem.*, 78, 8281–8289, 2006.

Deng, Z. Z., Zhao, C. S., Ma, N., Liu, P. F., Ran, L., Xu, W. Y., Chen, J., Liang, Z., Liang, S., Huang, M. Y., Ma, X. C., Zhang, Q., Quan, J. N., Yan, P., Henning, S., Mildenberger, K., Sommerhage, E., Schäfer, M., Stratmann, F., and Wiedensohler, A.: Size-resolved and bulk activation properties of aerosols in the North China Plain, *Atmos. Chem. Phys.*, 11, 3835–3846, doi:10.5194/acp-11-3835-2011, 2011.

Deng, Z. Z., Zhao, C. S., Ma, N., Ran, L., Zhou, G. Q., Lu, D. R., and Zhou, X. J.: An examination of parameterizations for the CCN number concentration based on in situ measurements of aerosol activation properties in the North China Plain, *Atmos. Chem. Phys.*, 13, 6227–6237, doi:10.5194/acp-13-6227-2013, 2013.

Dusek, U., Frank, G. P., Hildebrandt, L., Curtius, J., Schneider, J., Walter, S., Chand, D., Drewnick, F., Hings, S., Jung, D., Borrmann, S., and Andreae, M. O.: Size matters more than chemistry for cloud-nucleating ability of aerosol particles, *Science*, 312, 1375–1378, 2006.

Ervens, B., Cubison, M., Andrews, E., Feingold, G., Ogren, J. A., Jimenez, J. L., DeCarlo, P., and Nenes, A.: Prediction of cloud condensation nucleus number concentration using measurements of aerosol size distributions and composition and light scattering enhancement due to humidity, *J. Geophys. Res.*, 112, D10S32, doi:10.1029/2006JD007426, 2007.

Ervens, B., Cubison, M. J., Andrews, E., Feingold, G., Ogren, J. A., Jimenez, J. L., Quinn, P. K., Bates, T. S., Wang, J., Zhang, Q., Coe, H., Flynn, M., and Allan, J. D.: CCN predictions using simplified assumptions of organic aerosol composition and mixing state: a synthesis from

**Size-resolved CCN  
and HR-ToF-AMS  
measurements in  
Hong Kong**

J. W. Meng et al.

Title Page

Abstract

Introduction

Conclusions

References

Tables

Figures

◀

▶

◀

▶

Back

Close

Full Screen / Esc

Printer-friendly Version

Interactive Discussion

six different locations, *Atmos. Chem. Phys.*, 10, 4795–4807, doi:10.5194/acp-10-4795-2010, 2010.

Gong, Z., Lan, Z., Xue, L., Zeng, L., He, L., and Huang, X.: Characterization of submicron aerosols in the urban outflow of the central Pearl River Delta region of China, *Front. Environ. Sci. Eng.*, 6, 725–733, 2012.

Gunthe, S. S., King, S. M., Rose, D., Chen, Q., Roldin, P., Farmer, D. K., Jimenez, J. L., Artaxo, P., Andreae, M. O., Martin, S. T., and Pöschl, U.: Cloud condensation nuclei in pristine tropical rainforest air of Amazonia: size-resolved measurements and modeling of atmospheric aerosol composition and CCN activity, *Atmos. Chem. Phys.*, 9, 7551–7575, doi:10.5194/acp-9-7551-2009, 2009.

Gunthe, S. S., Rose, D., Su, H., Garland, R. M., Achtert, P., Nowak, A., Wiedensohler, A., Kuwata, M., Takegawa, N., Kondo, Y., Hu, M., Shao, M., Zhu, T., Andreae, M. O., and Pöschl, U.: Cloud condensation nuclei (CCN) from fresh and aged air pollution in the megacity region of Beijing, *Atmos. Chem. Phys.*, 11, 11023–11039, doi:10.5194/acp-11-11023-2011, 2011.

Hersey, S. P., Craven, J. S., Schilling, K. A., Metcalf, A. R., Sorooshian, A., Chan, M. N., Flanagan, R. C., and Seinfeld, J. H.: The Pasadena Aerosol Characterization Observatory (PACO): chemical and physical analysis of the Western Los Angeles basin aerosol, *Atmos. Chem. Phys.*, 11, 7417–7443, doi:10.5194/acp-11-7417-2011, 2011.

Huang, X. H., Bian, Q., Ng, W. M., Louie, P. K., and Yu, J. Z.: Characterization of PM<sub>2.5</sub> major components and source investigation in suburban Hong Kong: a one year monitoring study, *Aerosol Air Qual. Res.*, 14, 237–250, 2014.

Kammermann, L., Gysel, M., Weingartner, E., Herich, H., Cziczo, D. J., Holst, T., Svenningsson, B., Arneth, A., and Baltensperger, U.: Subarctic atmospheric aerosol composition: 3. measured and modeled properties of cloud condensation nuclei, *J. Geophys. Res.*, 115, D04202, doi:10.1029/2009JD012447, 2010.

Kerminen, V.-M., Paramonov, M., Anttila, T., Riipinen, I., Fountoukis, C., Korhonen, H., Asmi, E., Laakso, L., Lihavainen, H., Swietlicki, E., Svenningsson, B., Asmi, A., Pandis, S. N., Kulmala, M., and Petäjä, T.: Cloud condensation nuclei production associated with atmospheric nucleation: a synthesis based on existing literature and new results, *Atmos. Chem. Phys.*, 12, 12037–12059, doi:10.5194/acp-12-12037-2012, 2012.

Kim, J. H., Yum, S. S., Shim, S., Yoon, S.-C., Hudson, J. G., Park, J., and Lee, S.-J.: On aerosol hygroscopicity, cloud condensation nuclei (CCN) spectra and critical supersaturation mea-

**Size-resolved CCN  
and HR-ToF-AMS  
measurements in  
Hong Kong**

J. W. Meng et al.

Title Page

Abstract

Introduction

Conclusions

References

Tables

Figures

◀

▶

◀

▶

Back

Close

Full Screen / Esc

Printer-friendly Version

Interactive Discussion

sured at two remote islands of Korea between 2006 and 2009, *Atmos. Chem. Phys.*, 11, 12627–12645, doi:10.5194/acp-11-12627-2011, 2011.

King, S. M., Rosenoern, T., Shilling, J. E., Chen, Q., and Martin, S. T.: Cloud condensation nucleus activity of secondary organic aerosol particles mixed with sulfate, *Geophys. Res. Lett.*, 34, L24806, doi:10.1029/2007GL030390, 2007.

Lambe, A. T., Onasch, T. B., Massoli, P., Croasdale, D. R., Wright, J. P., Ahern, A. T., Williams, L. R., Worsnop, D. R., Brune, W. H., and Davidovits, P.: Laboratory studies of the chemical composition and cloud condensation nuclei (CCN) activity of secondary organic aerosol (SOA) and oxidized primary organic aerosol (OPOA), *Atmos. Chem. Phys.*, 11, 8913–8928, doi:10.5194/acp-11-8913-2011, 2011.

Lance, S., Nenes, A., Medina, J., and Smith, J. N.: Mapping the operation of the DMT continuous flow CCN counter, *Aerosol Sci. Tech.*, 40, 242–254, 2006.

Lance, S., Nenes, A., Mazzoleni, C., Dubey, M. K., Gates, H., Varutbangkul, V., Rissman, T. A., Murphy, S. M., Sorooshian, A., and Flagan, R. C.: Cloud condensation nuclei activity, closure, and droplet growth kinetics of Houston aerosol during the Gulf of Mexico Atmospheric Composition and Climate Study (GoMACCS), *J. Geophys. Res.*, 114, D00F15, doi:10.1029/2008JD011699, 2009.

Lathem, T. L. and Nenes, A.: Water vapor depletion in the DMT continuous-flow CCN chamber: Effects on supersaturation and droplet growth, *Aerosol Sci. Tech.*, 45, 604–615, 2011.

Lathem, T. L., Beyersdorf, A. J., Thornhill, K. L., Winstead, E. L., Cubison, M. J., Hecobian, A., Jimenez, J. L., Weber, R. J., Anderson, B. E., and Nenes, A.: Analysis of CCN activity of Arctic aerosol and Canadian biomass burning during summer 2008, *Atmos. Chem. Phys.*, 13, 2735–2756, doi:10.5194/acp-13-2735-2013, 2013.

Lee, B. P., Li, Y. J., Yu, J. Z., Louie, P. K., and Chan, C. K.: Physical and chemical characterization of ambient aerosol by HR-ToF-AMS at a suburban site in Hong Kong during springtime 2011, *J. Geophys. Res.-Atmos.*, 118, 8625–8639, doi:10.1002/jgrd.50658, 2013.

Li, Y. J., Lee, B. Y. L., Yu, J. Z., Ng, N. L., and Chan, C. K.: Evaluating the degree of oxygenation of organic aerosol during foggy and hazy days in Hong Kong using high-resolution time-of-flight aerosol mass spectrometry (HR-ToF-AMS), *Atmos. Chem. Phys.*, 13, 8739–8753, doi:10.5194/acp-13-8739-2013, 2013.

Low, R. D. H.: A generalized equation for the solution effect in droplet growth, *J. Atmos. Sci.*, 26, 608–611, 1969.

**Size-resolved CCN  
and HR-ToF-AMS  
measurements in  
Hong Kong**

J. W. Meng et al.

Title Page

Abstract

Introduction

Conclusions

References

Tables

Figures

◀

▶

◀

▶

Back

Close

Full Screen / Esc

Printer-friendly Version

Interactive Discussion

Massoli, P., Lambe, A. T., Ahern, A. T., Williams, L. R., Ehn, M., Mikkila, J., Canagaratna, M. R., Brune, W. H., Onasch, T. B., Jayne, J. T., Petaja, T., Kulmala, M., Laaksonen, A., Kolb, C. E., Davidovits, P., and Worsnop, D. R.: Relationship between aerosol oxidation level and hygroscopic properties of laboratory generated secondary organic aerosol (SOA) particles, *Geophys. Res. Lett.*, 37, L24801, doi:10.1029/2010gl045258, 2010.

Medina, J., Nenes, A., Sotiropoulou, R. E. P., Cottrell, L. D., Ziemba, L. D., Beckman, P. J., and Griffin, R. J.: Cloud condensation nuclei closure during the International Consortium for Atmospheric Research on Transport and Transformation 2004 campaign: effects of size-resolved composition, *J. Geophys. Res.*, 112, D10s31, doi:10.1029/2006jd007588, 2007.

Mei, F., Setyan, A., Zhang, Q., and Wang, J.: CCN activity of organic aerosols observed downwind of urban emissions during CARES, *Atmos. Chem. Phys.*, 13, 12155–12169, doi:10.5194/acp-13-12155-2013, 2013.

Moore, R. H., Cerully, K., Bahreini, R., Brock, C. A., Middlebrook, A. M., and Nenes, A.: Hygroscopicity and composition of California CCN during summer 2010, *J. Geophys. Res.-Atmos.*, 117, D00v12, doi:10.1029/2011jd017352, 2012a.

Moore, R. H., Nenes, A., and Medina, J.: Scanning mobility CCN analysis-A method for fast measurements of size-resolved CCN distributions and activation kinetics, *Aerosol Sci. Tech.*, 44, 861–871, 2010.

Moore, R. H., Raatikainen, T., Langridge, J. M., Bahreini, R., Brock, C. A., Holloway, J. S., Lack, D. A., Middlebrook, A. M., Perring, A. E., Schwarz, J. P., Spackman, J. R., and Nenes, A.: CCN spectra, hygroscopicity, and droplet activation kinetics of secondary organic aerosol resulting from the 2010 Deepwater Horizon oil spill, *Environ. Sci. Technol.*, 46, 3093–3100, 2012b.

Padró, L. T., Moore, R. H., Zhang, X., Rastogi, N., Weber, R. J., and Nenes, A.: Mixing state and compositional effects on CCN activity and droplet growth kinetics of size-resolved CCN in an urban environment, *Atmos. Chem. Phys.*, 12, 10239–10255, doi:10.5194/acp-12-10239-2012, 2012.

Padró, L. T., Tkacik, D., Lathem, T., Hennigan, C. J., Sullivan, A. P., Weber, R. J., Huey, L. G., and Nenes, A.: Investigation of cloud condensation nuclei properties and droplet growth kinetics of the water-soluble aerosol fraction in Mexico City, *J. Geophys. Res.-Atmos.*, 115, D09204, doi:10.1029/2009jd013195, 2010.

**Size-resolved CCN  
and HR-ToF-AMS  
measurements in  
Hong Kong**

J. W. Meng et al.

Title Page

Abstract

Introduction

Conclusions

References

Tables

Figures

◀

▶

◀

▶

Back

Close

Full Screen / Esc

Printer-friendly Version

Interactive Discussion

- Petters, M. D. and Kreidenweis, S. M.: A single parameter representation of hygroscopic growth and cloud condensation nucleus activity, *Atmos. Chem. Phys.*, 7, 1961–1971, doi:10.5194/acp-7-1961-2007, 2007.
- Petters, M. D. and Kreidenweis, S. M.: A single parameter representation of hygroscopic growth and cloud condensation nucleus activity – Part 3: Including surfactant partitioning, *Atmos. Chem. Phys.*, 13, 1081–1091, doi:10.5194/acp-13-1081-2013, 2013.
- Pringle, K. J., Tost, H., Pozzer, A., Pöschl, U., and Lelieveld, J.: Global distribution of the effective aerosol hygroscopicity parameter for CCN activation, *Atmos. Chem. Phys.*, 10, 5241–5255, doi:10.5194/acp-10-5241-2010, 2010.
- Roberts, G. C. and Nenes, A.: A continuous-flow streamwise thermal-gradient CCN chamber for atmospheric measurements, *Aerosol Sci. Tech.*, 39, 206–221, 2005.
- Rose, D., Gunthe, S. S., Mikhailov, E., Frank, G. P., Dusek, U., Andreae, M. O., and Pöschl, U.: Calibration and measurement uncertainties of a continuous-flow cloud condensation nuclei counter (DMT-CCNC): CCN activation of ammonium sulfate and sodium chloride aerosol particles in theory and experiment, *Atmos. Chem. Phys.*, 8, 1153–1179, doi:10.5194/acp-8-1153-2008, 2008.
- Rose, D., Nowak, A., Achtert, P., Wiedensohler, A., Hu, M., Shao, M., Zhang, Y., Andreae, M. O., and Pöschl, U.: Cloud condensation nuclei in polluted air and biomass burning smoke near the mega-city Guangzhou, China – Part 1: Size-resolved measurements and implications for the modeling of aerosol particle hygroscopicity and CCN activity, *Atmos. Chem. Phys.*, 10, 3365–3383, doi:10.5194/acp-10-3365-2010, 2010.
- Rose, D., Gunthe, S. S., Su, H., Garland, R. M., Yang, H., Berghof, M., Cheng, Y. F., Wehner, B., Achtert, P., Nowak, A., Wiedensohler, A., Takegawa, N., Kondo, Y., Hu, M., Zhang, Y., Andreae, M. O., and Pöschl, U.: Cloud condensation nuclei in polluted air and biomass burning smoke near the mega-city Guangzhou, China – Part 2: Size-resolved aerosol chemical composition, diurnal cycles, and externally mixed weakly CCN-active soot particles, *Atmos. Chem. Phys.*, 11, 2817–2836, doi:10.5194/acp-11-2817-2011, 2011.
- Stroud, C. A., Nenes, A., Jimenez, J. L., DeCarlo, P. F., Huffman, J. A., Bruintjes, R., Nemitz, E., Delia, A. E., Toohey, D. W., Guenther, A. B., and Nandi, S.: Cloud activating properties of aerosol observed during CELTIC, *J. Atmos. Sci.*, 64, 441–459, 2007.
- Sueper, D.: ToF-AMS data analysis software: <http://cires.colorado.edu/jimenez-group/ToFAMSResources/ToFSoftware/index.html> (last access: 1 June 2012), 2011.

**Size-resolved CCN  
and HR-ToF-AMS  
measurements in  
Hong Kong**

J. W. Meng et al.

Title Page

Abstract

Introduction

Conclusions

References

Tables

Figures

◀

▶

◀

▶

Back

Close

Full Screen / Esc

Printer-friendly Version

Interactive Discussion

Sullivan, R. C., Moore, M. J. K., Petters, M. D., Kreidenweis, S. M., Roberts, G. C., and Prather, K. A.: Effect of chemical mixing state on the hygroscopicity and cloud nucleation properties of calcium mineral dust particles, *Atmos. Chem. Phys.*, 9, 3303–3316, doi:10.5194/acp-9-3303-2009, 2009.

5 Takegawa, N., Miyakawa, T., Watanabe, M., Kondo, Y., Miyazaki, Y., Han, S., Zhao, Y., Van Pinxteren, D., Brüggemann, E., Gnauk, T., Herrmann, H., Xiao, R., Deng, Z., Hu, M., Zhu, T., and Zhang, Y.: Performance of an Aerodyne aerosol mass spectrometer (AMS) during intensive campaigns in China in the summer of 2006, *Aerosol Sci. Tech.*, 43, 189–204, 2009.

Tang, I. N. and Munkelwitz, H. R.: Water activities, densities, and refractive indices of aqueous sulfates and sodium nitrate droplets of atmospheric importance, *J. Geophys. Res.-Atmos.*, 99, 18801–18818, doi:10.1029/94jd01345, 1994.

10 Textor, C., Schulz, M., Guibert, S., Kinne, S., Balkanski, Y., Bauer, S., Berntsen, T., Berglen, T., Boucher, O., Chin, M., Dentener, F., Diehl, T., Easter, R., Feichter, H., Fillmore, D., Ghan, S., Ginoux, P., Gong, S., Grini, A., Hendricks, J., Horowitz, L., Huang, P., Isaksen, I., Iversen, I., Kloster, S., Koch, D., Kirkevåg, A., Kristjansson, J. E., Krol, M., Lauer, A., Lamarque, J. F., Liu, X., Montanaro, V., Myhre, G., Penner, J., Pitari, G., Reddy, S., Seland, Ø., Stier, P., Takemura, T., and Tie, X.: Analysis and quantification of the diversities of aerosol life cycles within AeroCom, *Atmos. Chem. Phys.*, 6, 1777–1813, doi:10.5194/acp-6-1777-2006, 2006.

15 Wang, J., Cubison, M. J., Aiken, A. C., Jimenez, J. L., and Collins, D. R.: The importance of aerosol mixing state and size-resolved composition on CCN concentration and the variation of the importance with atmospheric aging of aerosols, *Atmos. Chem. Phys.*, 10, 7267–7283, doi:10.5194/acp-10-7267-2010, 2010.

20 Wang, S. C. and Flagan, R. C.: Scanning electrical mobility spectrometer, *Aerosol Sci. Tech.*, 13, 230–240, 1990.

25 Wex, H., McFiggans, G., Henning, S., and Stratmann, F.: Influence of the external mixing state of atmospheric aerosol on derived CCN number concentrations, *Geophys. Res. Lett.*, 37, L10805, doi:10.1029/2010gl043337, 2010.

30 Xiao, R., Takegawa, N., Zheng, M., Kondo, Y., Miyazaki, Y., Miyakawa, T., Hu, M., Shao, M., Zeng, L., Gong, Y., Lu, K., Deng, Z., Zhao, Y., and Zhang, Y. H.: Characterization and source apportionment of submicron aerosol with aerosol mass spectrometer during the PRIDE-PRD 2006 campaign, *Atmos. Chem. Phys.*, 11, 6911–6929, doi:10.5194/acp-11-6911-2011, 2011.

Young, K. C. and Warren, A. J.: A reexamination of the derivation of the equilibrium supersaturation curve for soluble particles, *J. Atmos. Sci.*, 49, 1138–1143, 1992.

Zhang, Z., Engling, G., Lin, C.-Y., Chou, C. C.-K., Lung, S.-C. C., Chang, S.-Y., Fan, S., Chan, C.-Y., and Zhang, Y.-H.: Chemical speciation, transport and contribution of biomass burning smoke to ambient aerosol in Guangzhou, a mega city of China, *Atmos. Environ.*, 44, 3187–3195, 2010.

5

**Size-resolved CCN and HR-ToF-AMS measurements in Hong Kong**

J. W. Meng et al.

Title Page

Abstract

Introduction

Conclusions

References

Tables

Figures

◀

▶

◀

▶

Back

Close

Full Screen / Esc

Printer-friendly Version

Interactive Discussion



## Size-resolved CCN and HR-ToF-AMS measurements in Hong Kong

J. W. Meng et al.

**Table 1.** Statistics of the bulk  $N_{\text{CCN}}$  ( $\text{cm}^{-3}$ ) at four SS (%) showing the minimum, maximum, mean number concentration, the  $N_{\text{CCN}}/N_{\text{CN}}$  ratio, and standard deviation (SD). The last column shows the number of samples ( $n$ ) in this campaign.

SS (%)	Max		Min		Mean $\pm$ SD		$n$
	$N_{\text{CCN}}$ ( $\text{cm}^{-3}$ )	$N_{\text{CCN}}/N_{\text{CN}}$	$N_{\text{CCN}}$ ( $\text{cm}^{-3}$ )	$N_{\text{CCN}}/N_{\text{CN}}$	$N_{\text{CCN}}$ ( $\text{cm}^{-3}$ )	$N_{\text{CCN}}/N_{\text{CN}}$	
0.15	2815	0.54	33	0.03	$512 \pm 452$	$0.16 \pm 0.08$	319
0.35	8055	0.78	186	0.08	$1546 \pm 1137$	$0.48 \pm 0.14$	316
0.50	9156	0.82	210	0.12	$1815 \pm 1285$	$0.57 \pm 0.14$	326
0.70	9268	0.92	280	0.16	$2082 \pm 1484$	$0.65 \pm 0.14$	320

[Title Page](#)
[Abstract](#)
[Introduction](#)
[Conclusions](#)
[References](#)
[Tables](#)
[Figures](#)
[Back](#)
[Close](#)
[Full Screen / Esc](#)
[Printer-friendly Version](#)
[Interactive Discussion](#)

## Size-resolved CCN and HR-ToF-AMS measurements in Hong Kong

J. W. Meng et al.

**Table 2.** The average size-resolved mass concentrations ( $\mu\text{g m}^{-3}$ , Conc.) and volume fractions ( $f$ ) of chemical compositions from size-resolved AMS measurements during the foggy, hazy and the non-episode periods. Conc. and  $f$  were obtained by integrating over the size range ( $D_m$ ) from 42 nm to 1200 nm for Fig. 3a–c and from 42 nm to 200 nm for Fig. 3d–f. Data are shown as mean  $\pm$  standard deviations.

Period	Organics		Sulfate		Ammonium		Nitrate		Chloride	
	Conc.	$f$								
Foggy	1.60 $\pm$ 1.10	0.39 $\pm$ 0.12	4.86 $\pm$ 3.51	0.45 $\pm$ 0.10	1.33 $\pm$ 0.98	0.14 $\pm$ 0.04	0.18 $\pm$ 0.12	0.03 $\pm$ 0.00	0.03 $\pm$ 0.02	0.001 $\pm$ 0.00
Hazy	4.25 $\pm$ 2.52	0.57 $\pm$ 0.08	5.96 $\pm$ 4.36	0.29 $\pm$ 0.06	1.71 $\pm$ 1.22	0.08 $\pm$ 0.03	0.51 $\pm$ 0.27	0.06 $\pm$ 0.01	0.02 $\pm$ 0.01	0.002 $\pm$ 0.00
The rest	1.19 $\pm$ 0.71	0.47 $\pm$ 0.11	2.65 $\pm$ 1.86	0.37 $\pm$ 0.08	0.81 $\pm$ 0.55	0.12 $\pm$ 0.03	0.25 $\pm$ 0.15	0.04 $\pm$ 0.00	0.02 $\pm$ 0.01	0.002 $\pm$ 0.00

[Title Page](#)
[Abstract](#)
[Introduction](#)
[Conclusions](#)
[References](#)
[Tables](#)
[Figures](#)
[Back](#)
[Close](#)
[Full Screen / Esc](#)
[Printer-friendly Version](#)
[Interactive Discussion](#)

## Size-resolved CCN and HR-ToF-AMS measurements in Hong Kong

J. W. Meng et al.

Title Page

Abstract

Introduction

Conclusions

References

Tables

Figures

⏪

⏩

◀

▶

Back

Close

Full Screen / Esc

Printer-friendly Version

Interactive Discussion

**Table 3.** Methods used in  $N_{\text{CCN}}$  prediction.

Methods	Mixing state	Chemical composition	$\kappa_{\text{AMS}}$	$D_{50}$
I	Internal	Bulk AMS measurements	$\kappa_{\text{AMS}} = 0.1 \times f_{\text{org}} + 0.6 \times f_{\text{inorg}}$	Individual
II	Internal	Bulk AMS measurements	$\kappa_{\text{AMS}} = 0.1 \times f_{\text{org}} + 0.6 \times f_{\text{inorg}}$	Average
III	Internal	Size-resolved AMS measurements	$\kappa_{\text{AMS}} = 0.1 \times f_{\text{org}} + 0.6 \times f_{\text{inorg}}$	Individual
IV	Internal	Size-resolved AMS measurements	$\kappa_{\text{AMS}} = 0.1 \times f_{\text{org}} + 0.6 \times f_{\text{inorg}}$	Average
V	Internal	N/A	0.35/0.33/0.30	Constants

## Size-resolved CCN and HR-ToF-AMS measurements in Hong Kong

J. W. Meng et al.

Title Page

Abstract

Introduction

Conclusions

References

Tables

Figures

◀

▶

◀

▶

Back

Close

Full Screen / Esc

Printer-friendly Version

Interactive Discussion

**Table 4.** Overview of the  $N_{\text{CCN}}$  predictions,  $\kappa$  is shown as mean  $\pm$  standard deviation.

Categories	Principles	SS (%)	$\kappa$	Slope	$R^2$
CCN <sub>C</sub>	The average $D_{50}$ from CCN measurement	0.15	$0.39 \pm 0.06$	1.10	0.94
		0.35	$0.36 \pm 0.09$	1.01	0.95
		0.50	$0.31 \pm 0.10$	1.05	0.97
		0.70	$0.28 \pm 0.09$	1.08	0.98
	The average CCN activation ratio	0.15	–	1.09	0.94
		0.35	–	0.99	0.95
		0.50	–	1.02	0.97
		0.70	–	1.04	0.98
AMS	The $D_{50}$ from bulk $\kappa_{\text{AMS}}$	0.15	–	1.21	0.93
		0.35	–	1.06	0.95
		0.50	–	1.13	0.96
		0.70	–	1.17	0.98
	The average $D_{50}$ from bulk $\kappa_{\text{AMS}}$	0.15	$0.45 \pm 0.07$	1.26	0.93
		0.35	$0.46 \pm 0.06$	1.08	0.96
		0.50	$0.46 \pm 0.06$	1.13	0.96
		0.70	$0.46 \pm 0.07$	1.18	0.98
	The $D_{50}$ from size-resolved $\kappa_{\text{AMS}}$	0.15	–	1.06	0.91
		0.35	–	0.94	0.93
		0.50	–	1.03	0.95
		0.70	–	1.10	0.97
	The average $D_{50}$ from size-resolved $\kappa_{\text{AMS}}$	0.15	$0.37 \pm 0.07$	1.08	0.94
		0.35	$0.35 \pm 0.08$	1.01	0.95
		0.50	$0.31 \pm 0.07$	1.05	0.97
		0.70	$0.29 \pm 0.09$	1.09	0.98
Others	Constant $\kappa$	0.15	0.35/0.33/0.30	1.05/0.98/0.91	0.95/0.95/0.95
		0.35	0.35/0.33/0.30	1.01/0.96/0.91	0.95/0.95/0.95
		0.50	0.35/0.33/0.30	1.08/1.05/1.03	0.97/0.97/0.97
		0.70	0.35/0.33/0.30	1.13/1.12/1.11	0.98/0.98/0.98

## Size-resolved CCN and HR-ToF-AMS measurements in Hong Kong

J. W. Meng et al.

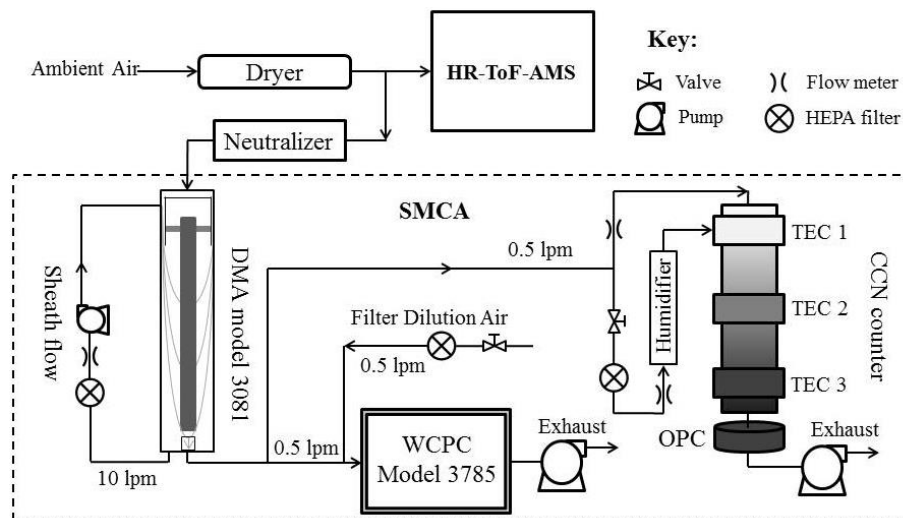


**Fig. 1.** Schematic of the experimental setup for size-resolved CCN activation and chemical composition measurement.

Title Page

Abstract

Introduction

Conclusions

References

Tables

Figures

⏪

⏩

⏴

⏵

Back

Close

Full Screen / Esc

Printer-friendly Version

Interactive Discussion

## Size-resolved CCN and HR-ToF-AMS measurements in Hong Kong

J. W. Meng et al.

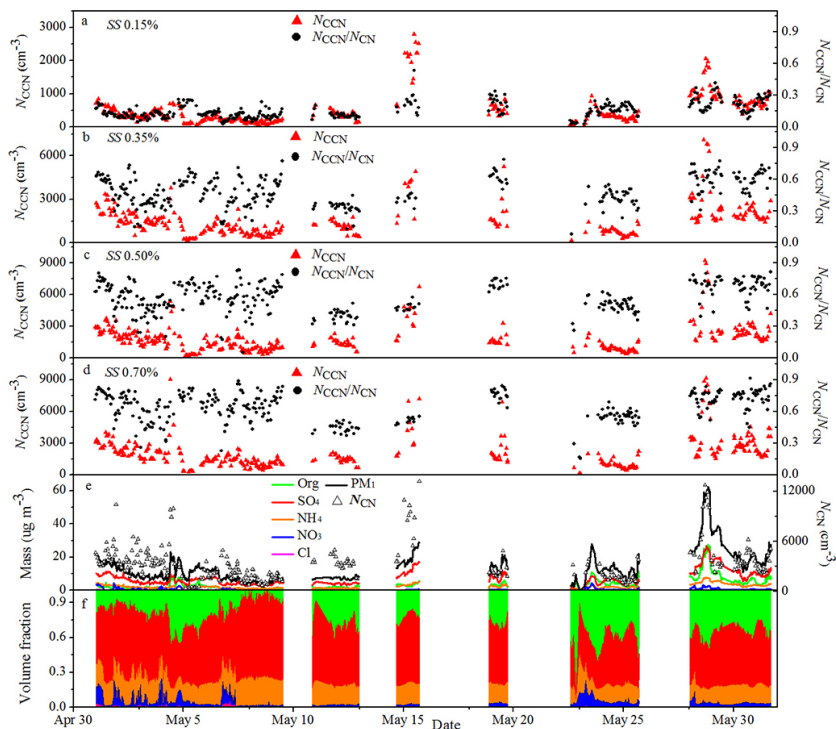


**Fig. 2.** The  $N_{CCN}$  and the  $N_{CCN}/N_{CN}$  ratio at SS of (a) 0.15 %, (b) 0.35 %, (c) 0.50 %, and (d) 0.70 %; (e)  $N_{CN}$  and NR-species mass concentrations from CCNc, SMPS and AMS; (f) NR-species volume fractions derived from AMS.

Title Page

Abstract

Introduction

Conclusions

References

Tables

Figures

◀

▶

◀

▶

Back

Close

Full Screen / Esc

Printer-friendly Version

Interactive Discussion

## Size-resolved CCN and HR-ToF-AMS measurements in Hong Kong

J. W. Meng et al.

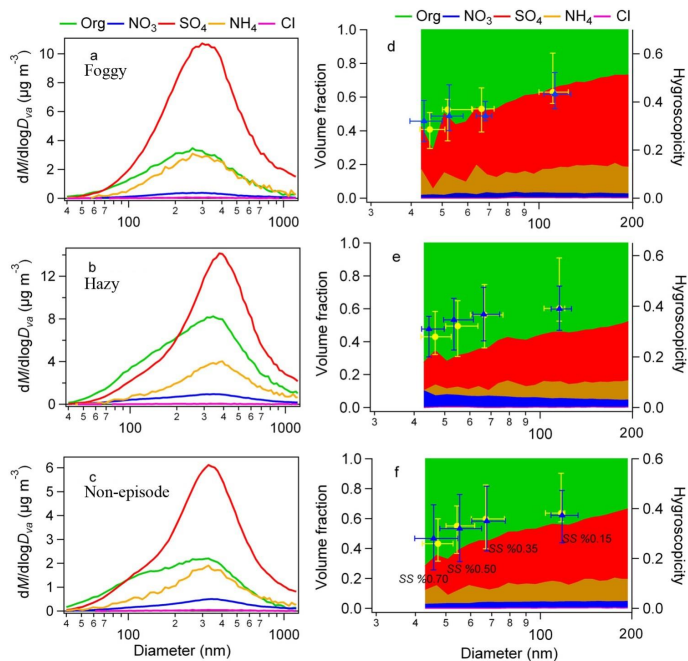


**Fig. 3.** Size-resolved mass concentration distributions of aerosol chemical composition derived from AMS averaged over (a) the foggy period, (b) the hazy period, and (c) the non-episode periods; the corresponding size-resolved volume fractions of aerosol chemical compositions (colored areas), the observed  $\kappa_{\text{CCN}}$  (yellow) and the calculated  $\kappa_{\text{AMS}}$  (blue) during (d) the foggy period, (e) the hazy period and (f) the non-episode period. Data points median values and interquartile ranges.  $\kappa_{\text{inorg}} = 0.6$  in all cases,  $\kappa_{\text{org}} = 0.1$  in (d) and (f),  $\kappa_{\text{org}} = 0.2$  in (e).

Title Page

Abstract

Introduction

Conclusions

References

Tables

Figures

◀

▶

◀

▶

Back

Close

Full Screen / Esc

Printer-friendly Version

Interactive Discussion

## Size-resolved CCN and HR-ToF-AMS measurements in Hong Kong

J. W. Meng et al.

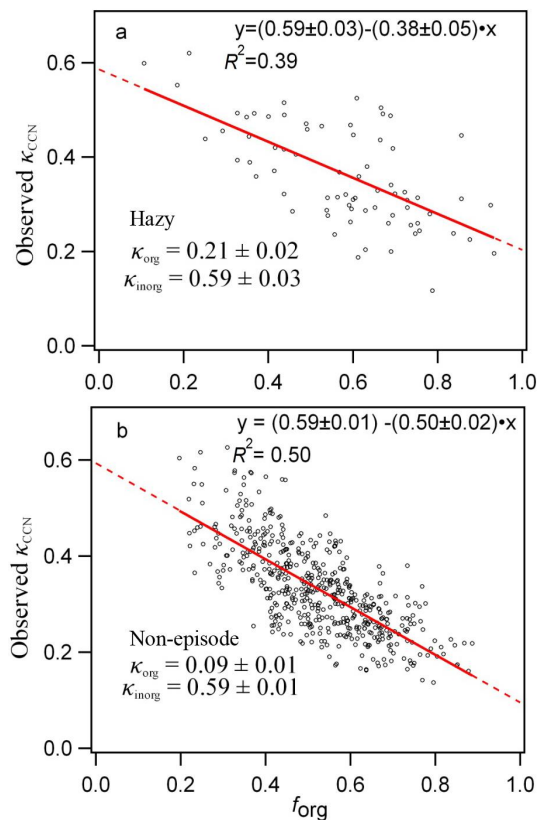


**Fig. 4.** Correlations between the observed  $\kappa_{\text{CCN}}$  and the organic volume fraction ( $f_{\text{org}}$ ) determined by size-resolved AMS measurements for the **(a)** hazy period ( $n = 72$ ) and **(b)** the non-episode period ( $n = 516$ ). The red line is the linear least squares fit shown in figure.

[Title Page](#)[Abstract](#)[Introduction](#)[Conclusions](#)[References](#)[Tables](#)[Figures](#)[◀](#)[▶](#)[◀](#)[▶](#)[Back](#)[Close](#)[Full Screen / Esc](#)[Printer-friendly Version](#)[Interactive Discussion](#)

## Size-resolved CCN and HR-ToF-AMS measurements in Hong Kong

J. W. Meng et al.

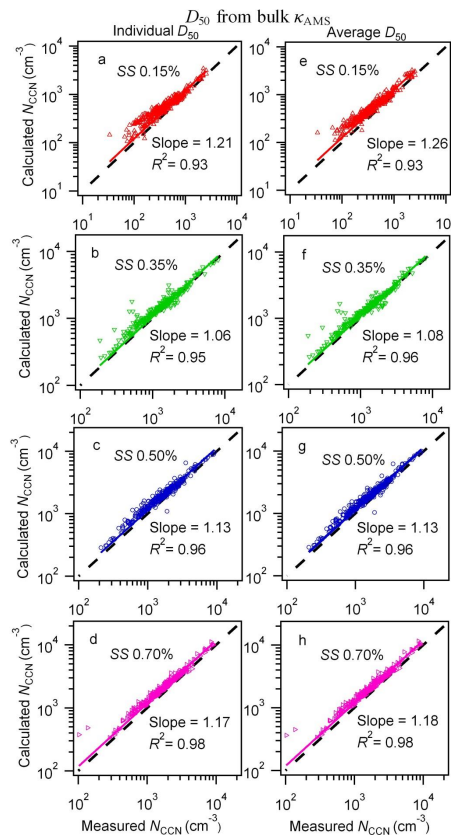


**Fig. 5.** Predictions of  $N_{\text{CCN}}$  based on (a–d) the individual  $D_{50}$  and (e–h) the average  $D_{50}$  over the whole period from the bulk  $\kappa_{\text{AMS}}$ .

Title Page

Abstract

Introduction

Conclusions

References

Tables

Figures

◀

▶

◀

▶

Back

Close

Full Screen / Esc

Printer-friendly Version

Interactive Discussion

## Size-resolved CCN and HR-ToF-AMS measurements in Hong Kong

J. W. Meng et al.

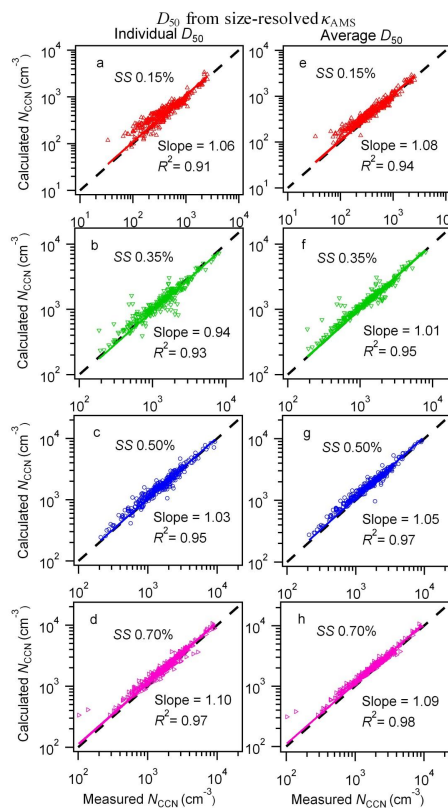


**Fig. 6.** Predictions of  $N_{\text{CCN}}$  based on (a–d) the individual  $D_{50}$  and (e–h) the average  $D_{50}$  over the whole period from the size-resolved  $\kappa_{\text{AMS}}$ .

Title Page

Abstract

Introduction

Conclusions

References

Tables

Figures

◀

▶

◀

▶

Back

Close

Full Screen / Esc

Printer-friendly Version

Interactive Discussion

## Size-resolved CCN and HR-ToF-AMS measurements in Hong Kong

J. W. Meng et al.

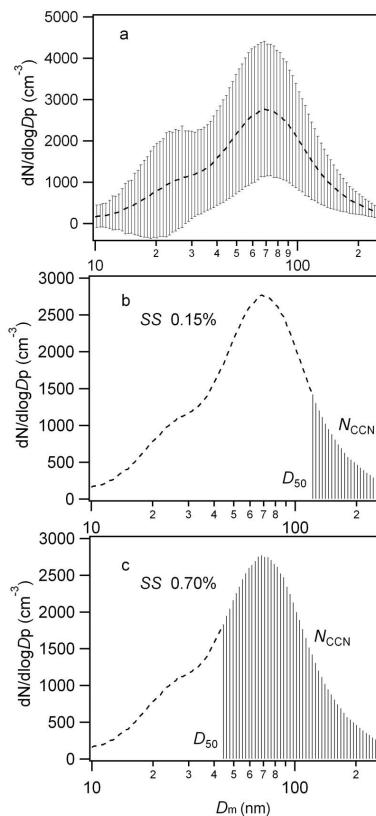


**Fig. 7.** The average aerosol size distribution over the whole period **(a)**,  $N_{\text{CCN}}$  prediction based on  $D_{50}$  at SS of **(b)** 0.15 % and **(c)** 0.70 %. Data points are mean values and standard deviation.

[Title Page](#)
[Abstract](#)
[Introduction](#)
[Conclusions](#)
[References](#)
[Tables](#)
[Figures](#)
[⏪](#)
[⏩](#)
[◀](#)
[▶](#)
[Back](#)
[Close](#)
[Full Screen / Esc](#)
[Printer-friendly Version](#)
[Interactive Discussion](#)

## Size-resolved CCN and HR-ToF-AMS measurements in Hong Kong

J. W. Meng et al.

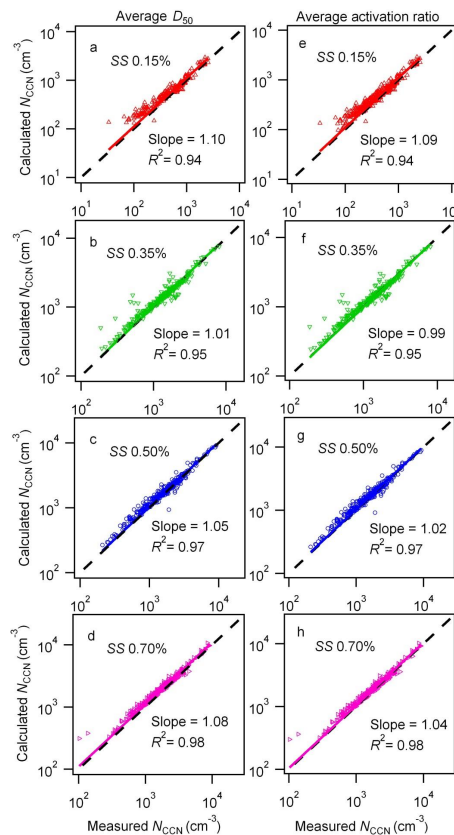


**Fig. 8.**  $N_{\text{CCN}}$  estimation in the whole period based on (a–d) the average  $D_{50}$  and (e–h) the average size-resolved CCN activation ratio from CCN measurement over the whole period.

[Title Page](#)
[Abstract](#)
[Introduction](#)
[Conclusions](#)
[References](#)
[Tables](#)
[Figures](#)
[◀](#)
[▶](#)
[◀](#)
[▶](#)
[Back](#)
[Close](#)
[Full Screen / Esc](#)
[Printer-friendly Version](#)
[Interactive Discussion](#)

## Size-resolved CCN and HR-ToF-AMS measurements in Hong Kong

J. W. Meng et al.

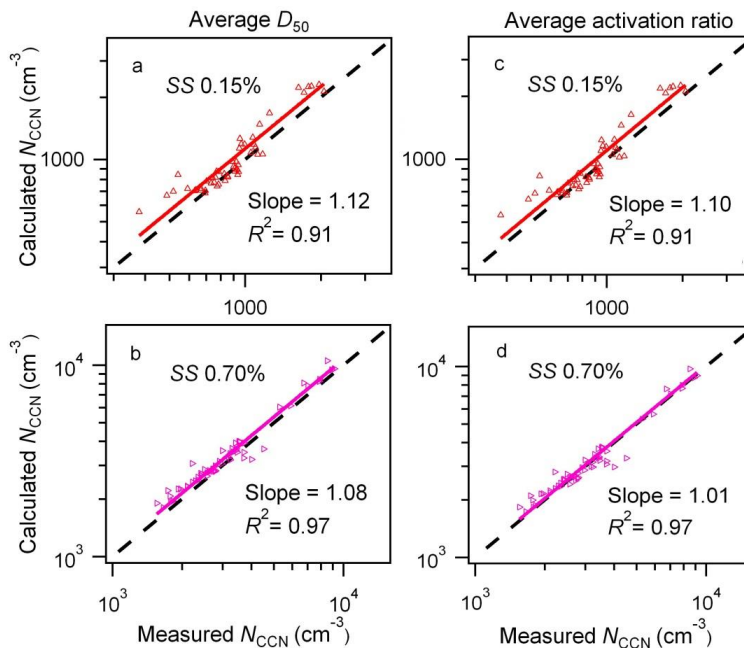


**Fig. 9.**  $N_{\text{CCN}}$  estimation in hazy period based on (a and b) the average  $D_{50}$  and (c and d) the average size-resolved CCN activation ratio from CCN measurement over the hazy period.